SURGERY

Clinical recovery from surgery correlates with single-cell immune signatures

Brice Gaudillière,[1,2]* Gabriela K. Fragiadakis,[2,3]* Robert V. Bruggner,[2,4] Monica Nicolau,[2,5,6] Rachel Finck,[2,3] Martha Tingle,[1] Julian Silva,[1] Edward A. Ganio,[1] Christine G. Yeh,[1] William J. Maloney,[7] James I. Huddleston,[7] Stuart B. Goodman,[7] Mark M. Davis,[3] Sean C. Bendall,[2,3] Wendy J. Fantl,[2,3,8] Martin S. Angst,[1†‡] Garry P. Nolan[2,3†‡]

Delayed recovery from surgery causes personal suffering and substantial societal and economic costs. Whether immune mechanisms determine recovery after surgical trauma remains ill-defined. Single-cell mass cytometry was applied to serial whole-blood samples from 32 patients undergoing hip replacement to comprehensively characterize the phenotypic and functional immune response to surgical trauma. The simultaneous analysis of 14,000 phosphorylation events in precisely phenotyped immune cell subsets revealed uniform signaling responses among patients, demarcating a surgical immune signature. When regressed against clinical parameters of surgical recovery, including functional impairment and pain, strong correlations were found with STAT3 (signal transducer and activator of transcription), CREB (adenosine 3′,5′-monophosphate response element–binding protein), and NF-κB (nuclear factor κB) signaling responses in subsets of $CD14^+$ monocytes (R = 0.7 to 0.8, false discovery rate <0.01). These sentinel results demonstrate the capacity of mass cytometry to survey the human immune system in a relevant clinical context. The mechanistically derived immune correlates point to diagnostic signatures, and potential therapeutic targets, that could postoperatively improve patient recovery.

INTRODUCTION

More than 100 million surgeries are performed annually in Europe and the United States (*1*). This number is expected to grow as the population ages. Convalescence after surgery is highly variable, and protracted recovery results in personal suffering, functional impairment, delayed return to work, and substantial societal and economic costs (*2*). Recent work anchored in concept analysis defined postoperative recovery as the "process to regain control over physical, psychological, social and habitual functions, and return to preoperative levels of independence and psychological well-being" (*3*). This definition reflects a shift from traditional recovery parameters, such as length of hospital stay, to patient-centered outcomes including absence of symptoms, the ability to perform regular activities, return to work, and regain quality of life (*4*). In this context, major determinants of protracted recovery are fatigue, pain, and resulting functional impairment (*5*, *6*). Fatigue is a key sickness behavior and is described as "an indefinable weakness throughout the body requiring sitting or lying down after minor tasks."

Perioperative care now includes enhanced recovery protocols and evidence-based practice guidelines largely anchored in observational data (*7*). Although these protocols have reduced length of hospital stay, their impact on recovery after hospital discharge and the elements of these protocols that may contribute to improved recovery are uncertain. Similarly, the physiologic and mechanistic underpinnings of surgical recovery remain a "black box" phenomenon. Understanding the mechanisms that drive recovery after surgery will advance therapeutic strategies and allow patient-specific tailoring of recovery protocols. Considering that profound immune perturbations occur in response to surgery, comprehensive and longitudinal characterization of the human immune system in patients undergoing surgery is foundational for gaining such mechanistic insight.

Traumatic injury initiates an intricate programmed immune response (*8*): Hours after severe trauma, neutrophils and monocytes are rapidly activated and recruited to the periphery by damage response antigens, alarmins (for example, HMGB1), and increased levels of tumor necrosis factor–α (TNF-α), interleukin-1β (IL-1β), and IL-6 (*9*–*11*). This is followed by a compensatory phase characterized by decreased numbers of T cell subsets (*12*). The various immune cell types are thought to integrate multiple environmental signals into cohesive signaling responses that enable wound healing and recovery. A recent genome-wide analysis of pooled circulating leukocytes revealed that traumatic injury organized more than 80% of the leukocyte transcriptome according to cell type–specific signaling pathways (*13*).

The profound inflammatory response to tissue injury has prompted a long-standing interest in unraveling immune mechanisms that determine recovery after surgical trauma (*14*). The severity of surgical trauma relates to the magnitude of the immune response, which may in turn influence postoperative outcomes (*15*). Previous studies have focused on secreted humoral factors (*11*, *16*), distribution patterns of immune cell subsets (*10*, *17*), and genomic analysis of pooled circulating leukocytes (*13*). These reports provided insight into aspects that govern the inflammatory response to traumatic injury but did not reveal strong correlations with clinical recovery. Although weak correlates to clinical outcomes were reported, none of these studies measured immune functional responses at the single-cell level, and strong signals might have gone undetected as specific immune cell subsets would have been functionally and phenotypically undercharacterized.

[1]Department of Anesthesiology, Perioperative and Pain Medicine, Stanford University School of Medicine, Stanford, CA 94305, USA. [2]Baxter Laboratory in Stem Cell Biology, Stanford University, Stanford, CA 94305, USA. [3]Department of Microbiology and Immunology, Stanford University, Stanford, CA 94305, USA. [4]Biomedical Informatics Program, Stanford University, Stanford, CA 94305, USA. [5]Department of Mathematics, Stanford University, Stanford, CA 94305, USA. [6]Center for Cancer Systems Biology, Stanford University, Stanford, CA 94305, USA. [7]Department of Orthopedic Surgery, Stanford University, Redwood City, CA 94063, USA. [8]Department of Obstetrics and Gynecology, Stanford University, Stanford, CA 94305, USA.
*These authors contributed equally to this work.
†These authors contributed equally to this work.
‡Corresponding author. E-mail: ang@stanford.edu (M.S.A.); gnolan@stanford.edu (G.P.N.)

Here, mass cytometry, a highly parameterized single cell–based platform that can determine functional responses in precisely phenotyped immune cell subsets (*18*–*20*), was used to comprehensively characterize phenotypic and functional alterations of the human immune system as they occur in vivo in patients undergoing major surgery. The primary aim was to extract "surgery" or "trauma-specific" immune signatures and to determine, secondarily, whether such signatures contain clinical correlates of surgical recovery.

RESULTS

Mass cytometry enables the detection of surgery-induced immune perturbations in clinical samples

On the basis of a premise that surgical intervention, or "trauma," acts as a systemic perturbation on multiple physiologic processes in the body, cell subsets based on traditional surface marker phenotyping were analyzed simultaneously with intracellular signaling cascades downstream of activated receptors. Whole peripheral blood was collected from primary hip arthroplasty (PHA) patients and, critically, was processed within 30 min to remain as close as possible to in vivo conditions. In a preliminary phase, samples from one patient collected 1 hour before and 1 and 24 hours after surgery were assayed in triplicate to determine whether trauma-induced changes in immune cell frequencies and intracellular signaling responses (phosphorylation of signaling proteins) could reliably be detected with mass cytometry (fig. S1). The sensitivity and specificity of all phospho-specific antibodies used in the assay were validated in vitro in whole-blood samples stimulated with a series of ligands known to induce the phosphorylation of signaling proteins included in the analysis (fig. S1B). Reproducible changes were observed for cell frequencies and intracellular signaling responses, validating the assay for subsequent studies (fig. S1).

In a pilot study of six PHA patients (fig. S2), whole-blood samples were collected 1 hour before and 1 hour, 24 hours, 72 hours, and 6 weeks after surgery. Samples were stained with antibodies recognizing 21 cell surface proteins and phosphoepitopes of 10 intracellular proteins, and

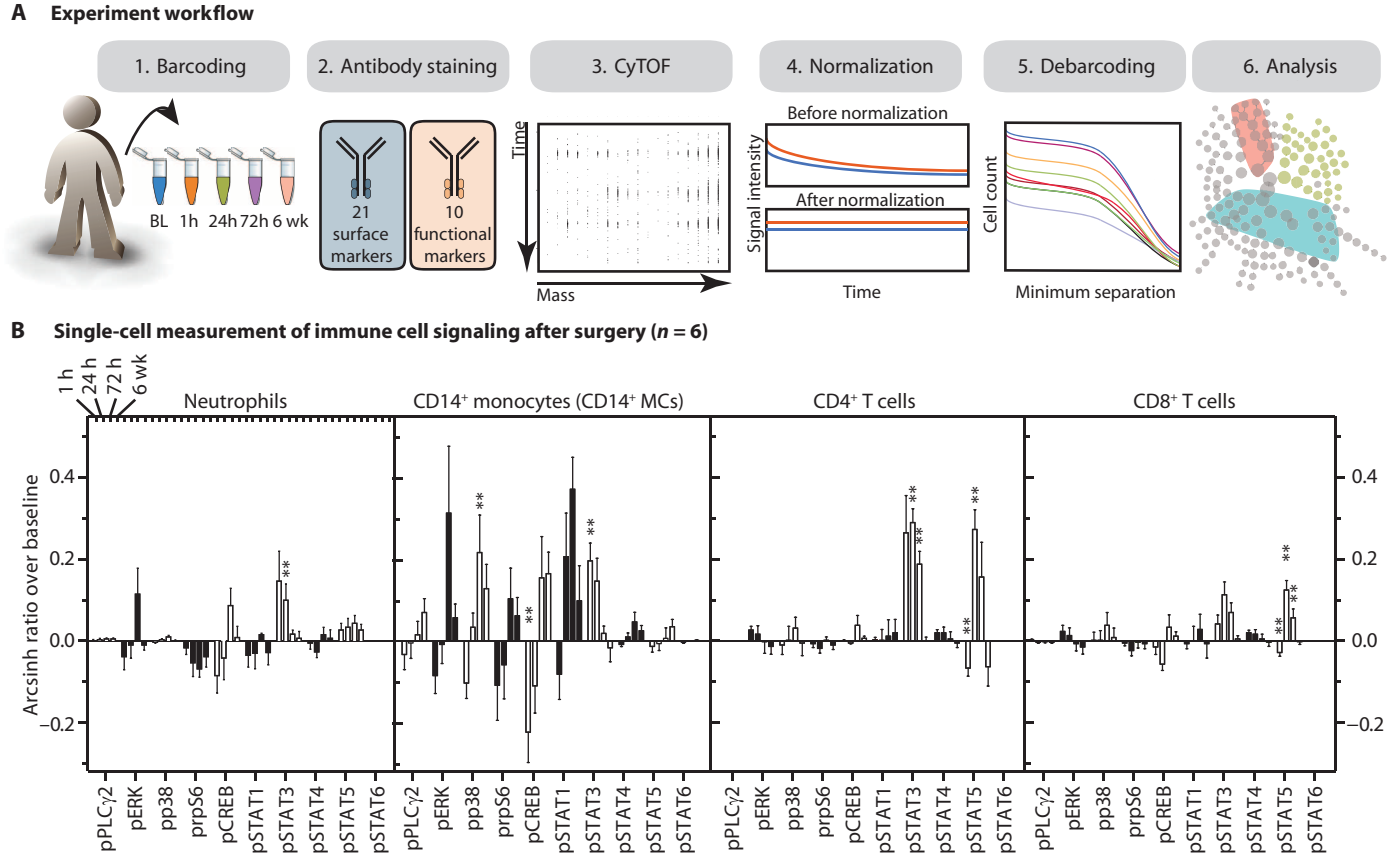

Fig. 1. Mass tag barcoding enables the longitudinal analysis of the cellular immune response in peripheral blood of patients undergoing surgery. (**A**) Experimental workflow. Whole-blood samples from six patients undergoing PHA were collected 1 hour before surgery [baseline (BL)] and 1 hour, 24 hours, 72 hours, and 6 weeks after surgery. After red blood cell lysis, leukocyte samples from each patient were barcoded using a unique combination of palladium isotopes (panel 1). Barcoded samples were pooled, stained with a panel of 31 antibodies (panel 2, table S1), and analyzed by mass cytometry (panel 3). Raw mass cytometry data were normalized for signal variation over time (*21*) (panel 4), debarcoded (*19*) (panel 5), and analyzed (panel 6). (**B**) Assay validation in surgical patients. Ten intracellular signaling responses to surgery were quantified for four immune cell subsets (neutrophils, $CD14^+$ MCs, $CD4^+$ T cells, and $CD8^+$ T cells). Signal induction for each signaling molecule was calculated as the difference of inverse hyperbolic sine medians between samples obtained at baseline and at 1 hour, 24 hours, 72 hours, and 6 weeks after surgery ("arcsinh ratio"). Five of 10 phosphoproteins (pSTAT1, pSTAT3, pSTAT5, pCREB, and pp38) displayed reproducible changes at 1, 24, or 72 hours after surgery compared to baseline. Results are means ± SEM. SAM two-class paired was used for statistical analysis [** indicates a false discovery rate (FDR) $q < 0.01$, $n = 6$].

processed for mass cytometry (*20*) (Fig. 1A and table S1). Substantial effort was undertaken to protect against potential batch effect and minimize signal variation because of sample processing. Each time series was barcoded using a combination of stable isotope mass tags (*19*) and processed simultaneously, and for each time point, reported frequencies and signaling responses were normalized to their measurements in the patient's baseline sample. Samples were also normalized for signal variation over machine time using normalization beads containing known concentration of metal isotopes, as described by Finck *et al.* (*21*).

Analysis initially focused on neutrophils, $CD14^+$ monocytes ($CD14^+$ MCs), and $CD4^+$ and $CD8^+$ T cells (figs. S3 and S4). Consistent with previous reports (*10*, *12*, *22*), surgery induced a 1.2-fold (±0.06, $q < 0.01$) expansion of neutrophils 1 hour after surgery, a 1.9-fold (±0.19, $q < 0.01$) expansion of $CD14^+$ MCs at 24 hours, and a contraction of $CD4^+$ and $CD8^+$ T cells to 0.77-fold (±0.07, $q < 0.01$) and 0.71-fold (±0.07, $q < 0.01$), respectively, at 24 hours (fig. S4). Intracellular signaling responses, indicated by changes in phosphorylation of signal transducer and activator of transcription 1 (STAT1), STAT3, STAT5, adenosine 3′,5′-monophosphate response element–binding protein (CREB), and p38, were induced in time- and cell type–specific manners (Fig. 1B, $q < 0.01$). Six weeks after surgery, cell subset frequencies and magnitudes of phosphosignals did not differ from presurgical values ($q > 0.05$), indicating restoration of immune homeostasis.

$CD33^+CD11b^+CD14^+HLA\text{-}DR^{low}$ monocytes expand sixfold after surgery

Having established that mass cytometry enabled the detection of surgery-induced perturbations in cell frequency and signaling, an observational study was conducted in 26 patients undergoing PHA to prospectively validate observed cellular responses to surgical trauma and to identify immune correlates of surgical recovery (fig. S2 and Table 1). All patients carried the primary diagnosis of nontraumatic osteoarthritis. Hip arthroplasties were performed using a standard lateral approach. Exclusion criteria included patients with any systemic disease or medication that might compromise the immune system (including recent infections; autoimmune disease; diagnosis of cancer, renal, hepatic, cardiovascular, and respiratory disease resulting in functional impairment; history of substance abuse; or chronic opioid therapy).

Serial blood samples and longitudinal data on clinical recovery were captured over a 6-week period. Whole-blood samples were barcoded, stained using the antibody panel in table S1 (right panel), and processed by mass cytometry as described in the pilot study. The frequencies of neutrophils, $CD14^+$ MCs, classical dendritic cells (cDCs), plasmacytoid dendritic cells (pDCs), natural killer (NK) cells, B cells, and $CD4^+$ and $CD8^+$ T cells were determined by manual gating (*23*) (Fig. 2A and fig. S3). Consistent with results from previous reports and the pilot study, NK cells [1.6-fold (±0.15, $q < 0.01$)] and neutrophils [1.3-fold (±0.04, $q < 0.01$)] expanded 1 hour after surgery. $CD14^+$ MCs expanded 2.4-fold (±0.29, $q < 0.01$) and 1.8-fold (±0.16, $q < 0.01$) at 24 and 72 hours, respectively. Mobilization of the myeloid compartment was followed by a contraction at 24 hours of $CD4^+$ and $CD8^+$ T cells to 0.76-fold (±0.04, $q < 0.01$) and 0.72-fold (±0.03, $q < 0.01$), respectively, that became less pronounced at 72 hours (0.88 ± 0.04 and 0.85 ± 0.03, respectively, $q < 0.01$). Consistent with pilot results, cell type frequencies 6 weeks after surgery were similar to presurgical values ($q > 0.05$).

A major advantage afforded by high-dimensional multiparameter data analyses lies in the ability to detect finely tuned cell subsets with

Table 1. Demographic and clinical variables ($N = 26$). SRS, Surgical Recovery Scale; WOMAC, Western Ontario and McMaster Universities Arthritis Index; SF-36, Short Form Health Survey; PCS, Physical Component Score; MCS, Mental Component Score; BDI, Beck Depression Inventory; POMS-A, Profile of Moods States Tension-Anxiety Scale; MAC, minimal alveolar concentration of average exposure during surgery.

Demographics*		
Gender (male/female)	16/10	
Race (Caucasian/African American)	25/1	
Age (years)	59.5 (54.0–68.0)	
Body mass index (kg/m^2)	26.5 (24.4–28.1)	
Questionnaires	**Before surgery**	**6 weeks after surgery**
SRS	62.3 (57.3–80.8)	80.8 (67.1–86.8)
WOMAC	131.5 (80.0–180.0)	33.5 (11.0–51.0)
SF-36		
PCS	38.9 (21.9–42.1)	41.5 (31.1–49.8)
MCS	55.3 (39.7–59.6)	60.3 (49.3–64.3)
BDI	7.5 (3.0–11.0)	5.5 (1.0–8.0)
POMS-A		
Men	5.5 (3.5–9.5)	5.0 (4.0–6.8)
Women	7.0 (5.0–14.0)	4.0 (3.0–4.0)
Surgery		
Duration (min)	100 (85–119)	
Blood loss (ml)	250 (200–310)	
Urine output (ml)	200 (100–300)	
Fluids		
Crystalloids (ml)	1500 (1000–2000)	
Colloids (ml)	0 (0–0)	
Blood products (ml)	0 (0–0)	
Time to discharge (days)	3.1 (3.0–3.8)	
Anesthesia		
Technique		
General (number of patients)	6	
Spinal (number of patients)	1	
General + spinal (number of patients)	19	
Volatile anesthetic		
Number of patients	25	
MAC (%)	0.5 (0.4–0.7)	
Nitrous oxide		
Number of patients	11	
MAC (%)	0.5 (0.4–0.6)	
Intrathecal medications		
Number of patients (%)	20	
Bupivacaine (mg)	11.3 (10.5–12.0)	
Morphine (mg)	0.2 (0.1–0.2)	
Opioid use†		
Intraoperative (mg)	2.8 (1.5–3.8)	
During hospital stay (mg)	16.0 (13.1–27.4)	
After discharge (mg)	9.0 (5.5–16.9)	

*Values indicate number of patients or median and interquartile range. †Milligram equivalent of intravenous hydromorphone. Dose during hospitalization is total cumulative dose. Dose after discharge is cumulative dose taken on survey days.

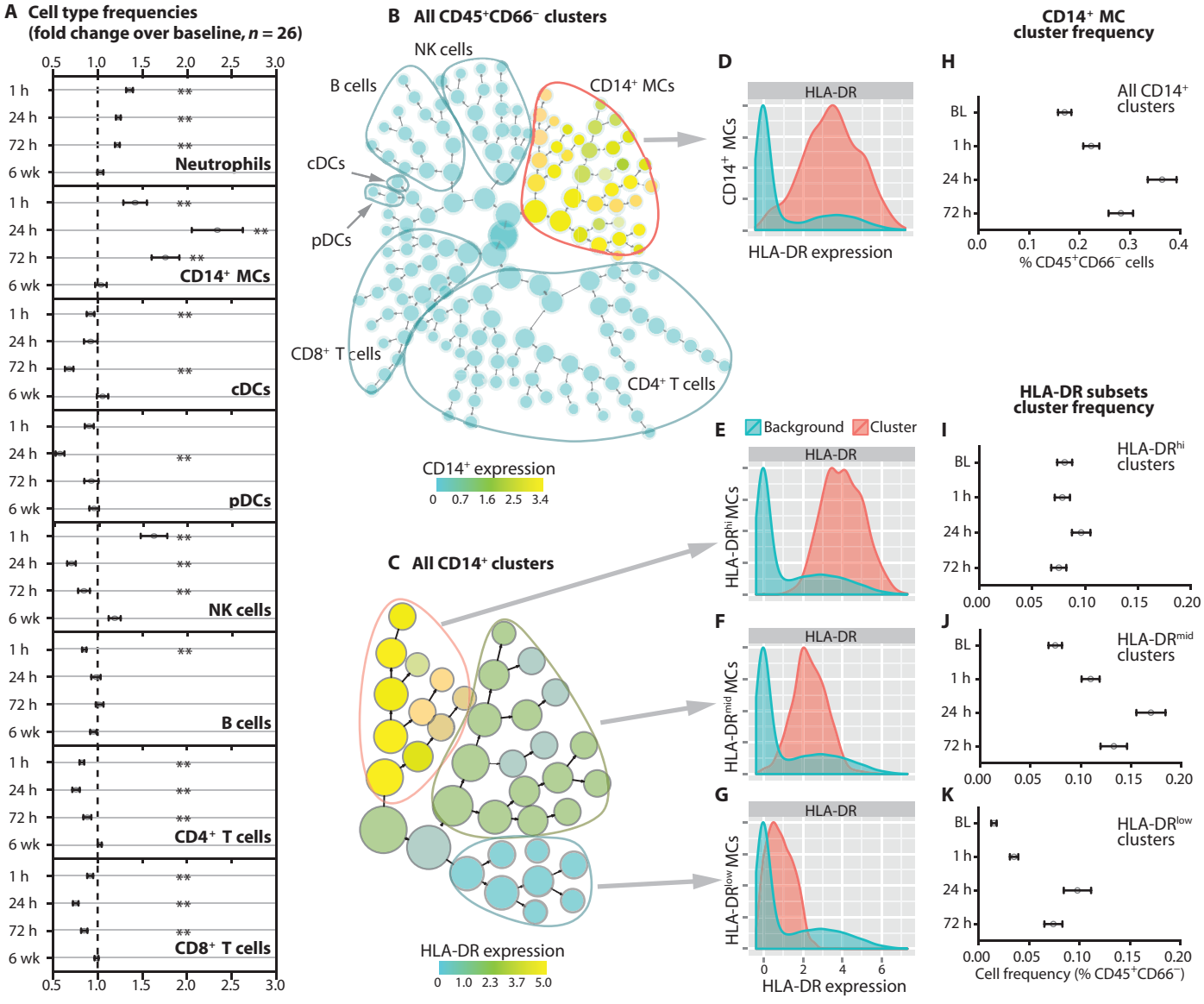

Fig. 2. Surgery induces a redistribution of major immune cell types and a sixfold expansion of HLA-DR^{low} CD14$^+$ MCs. (**A**) Frequencies of neutrophils, CD14$^+$ MCs, cDCs, pDCs, NK cells, B cells, CD4$^+$ T cells, and CD8$^+$ T cells are depicted for 26 patients 1 hour, 24 hours, 72 hours, and 6 weeks after surgery. Cell types were identified by manual gating (fig. S3). Neutrophil frequency was quantified as percent of total hematopoietic cells (CD61$^-$CD235$^-$). All other cell frequencies are expressed as percent total of mononuclear cells (CD45$^+$CD66$^-$). ** represents $q < 0.01$, $n = 26$, SAM two-class paired. Results are mean fold change ± SEM. (**B**) Visual representation of unsupervised hierarchical clustering. Results are shown for CD45$^+$CD66$^-$ immune cells. The analysis used 21 cell surface markers (table S1). Major immune cell compartments are contoured on the basis of expression of canonical lineage markers (fig. S5). Contoured in red are CD14$^+$ MCs. The color scale indicates median intensity of CD14 expression. Node sizes are scaled on the basis of frequency of cells in each cluster. (**C**) CD14$^+$ MCs were clustered into HLA-DR^{hi} (yellow), HLA-DR^{mid} (green), and HLA-DR^{low} (blue) subsets. The color scale indicates the median intensity of HLA-DR expression. (**D** to **G**) Histogram plots. Arrows designate histograms of HLA-DR expression for CD14$^+$ MC clusters (red) against HLA-DR background expression in all CD45$^+$CD66$^-$ cells (blue). (**H** to **K**) CD14$^+$ MC cell cluster frequencies 1 hour before and 1, 24, and 72 hours after surgery. Shown are frequencies of all CD14$^+$ MC clusters (H), HLA-DR^{hi} (I), HLA-DR^{mid} (J), and HLA-DR^{low} (K) CD14$^+$ MC clusters. Results are mean fold change ± SEM.

signaling changes that would be undetected in low parameter space. An unsupervised clustering algorithm was applied to comprehensively explore surgery-induced changes in cell subsets that may have been overlooked by manual gating strategies (*24*). The algorithm distills multidimensional single-cell data to a hierarchy of related clusters on the basis of cell surface markers (Fig. 2B and fig. S5). Cluster-specific analysis of cell frequency changes revealed that clusters within the CD45$^+$CD66$^-$CD3$^-$CD19$^-$CD33$^+$CD11b$^+$CD14$^+$ compartment (CD14$^+$ MC clusters) expanded fourfold (±0.28) after surgery, more than any other cell cluster (fig. S6). Expression of the human leukocyte antigen (HLA)–DR antigen partitioned CD14$^+$ MC clusters into HLA-DR^{hi}, HLA-DR^{mid}, and HLA-DR^{low} compartments (Fig. 2, C to G). Quantification of CD14$^+$ MC cluster frequencies showed that the HLA-DR^{mid} and HLA-DR^{low} compartments accounted for 49 and 45% of the CD14$^+$ MC cluster

expansion (Fig. 2, H to K). Notably, $CD33^+CD11b^+CD14^+HLA\text{-}DR^{low}$ monocytes expanded sixfold after surgery and had phenotypic similarity to myeloid-derived suppressor cells (MDSCs), previously described in the context of human malignancies as inhibitors of the adaptive immune system (*25*). Results of this unsupervised, high parameter analysis expand previous reports on monocytic HLA-DR expression after surgery (*26*). The current results underscore an unequivocal role of $HLA\text{-}DR^{mid}$ and $HLA\text{-}DR^{low}$ $CD14^+$ MCs in the surgical immune response because this approach enabled quantitative comparison among cell subsets within the broader context of the immune system.

STAT3, CREB, and NF-κB signaling pathways are differentially activated in $CD14^+$ MCs in response to surgery

A visual synopsis of surgery-induced changes in the phosphorylation states of 11 intracellular signaling proteins across eight different immune cell subsets, at four time points, and in 26 patients is shown (Fig. 3A). Significance analysis of microarray (SAM) (*27*) revealed 135 significant immune signaling responses to surgery ($q < 0.01$) with cell type–specific distributions across major hematopoietic lineages (Fig. 3B). Notably, 97% of all phospho-signals detected 1 hour before and 6 weeks after surgery were of similar magnitude ($q > 0.05$), underscoring the tight regulation of the immune system and its ability to restore homeostasis (Fig. 3B).

Between 1 and 72 hours after surgery, time-dependent signaling responses were detected in all immune cell types (table S2). Signaling changes were most pronounced in $CD14^+$ MCs and $CD4^+$ T cells (Fig. 3B and fig. S7). Sequential activation of STAT3 and STAT1 characterized the STAT response in $CD14^+$ MCs, whereas activation of STAT3 and STAT5 characterized the STAT response in $CD4^+$ T cells. Activation of STAT3 and STAT5 in $CD4^+$ T cells was detected at 1 hour; the highest level of activity of STAT3 in $CD14^+$ MCs was observed at this time point. Activity of STAT3 and STAT5 was less pronounced in $CD8^+$ than $CD4^+$ T cells but followed a similar pattern. Results indicate early and concurrent activation of major signaling pathways in innate and adaptive immune cell compartments. This challenges the conventional view that innate and adaptive immune responses to surgical trauma follow a sequential temporal pattern.

Further investigation of signaling responses in $CD14^+$ MCs revealed significant dephosphorylation of extracellular signal–regulated kinase (ERK), p38, MAPKAPK2 (MK2), p90RSK, rpS6, CREB, and nuclear factor κB (NF-κB) (p65-RelA) at 1 hour after surgery (Fig. 3, A and B, and fig. S7). By 72 hours, phosphorylation of these proteins had either returned to or exceeded baseline values. To characterize the signaling network underlying these coordinated phosphorylation patterns, correlation analysis was performed (Fig. 3C). Clustering of the resultant correlation coefficients revealed four modules that were preserved in all patients at all time points after surgery (Fig. 3, D and E, and fig. S8). Module 1 consisted of pNF-κB, pCREB, and prpS6, and module 2 consisted of pp38, pMAPKAPK2, pERK, and pp90RSK. Each of these proteins can be activated downstream of Toll-like receptors (TLRs) known to play an essential role in the innate response to sterile inflammation (*28*, *29*). Module 1 also included STAT1, possibly reflecting the indirect regulation of STAT1 downstream of TLR4 (*30*). Module 3 consisted of pSTAT5 and pPLCγ2, suggestive of coordinated activations of parallel signaling pathways not previously shown to cross-communicate (*31*, *32*), which warrants further investigation. Module 4 consisted only of pSTAT3 and was anti-correlated with other

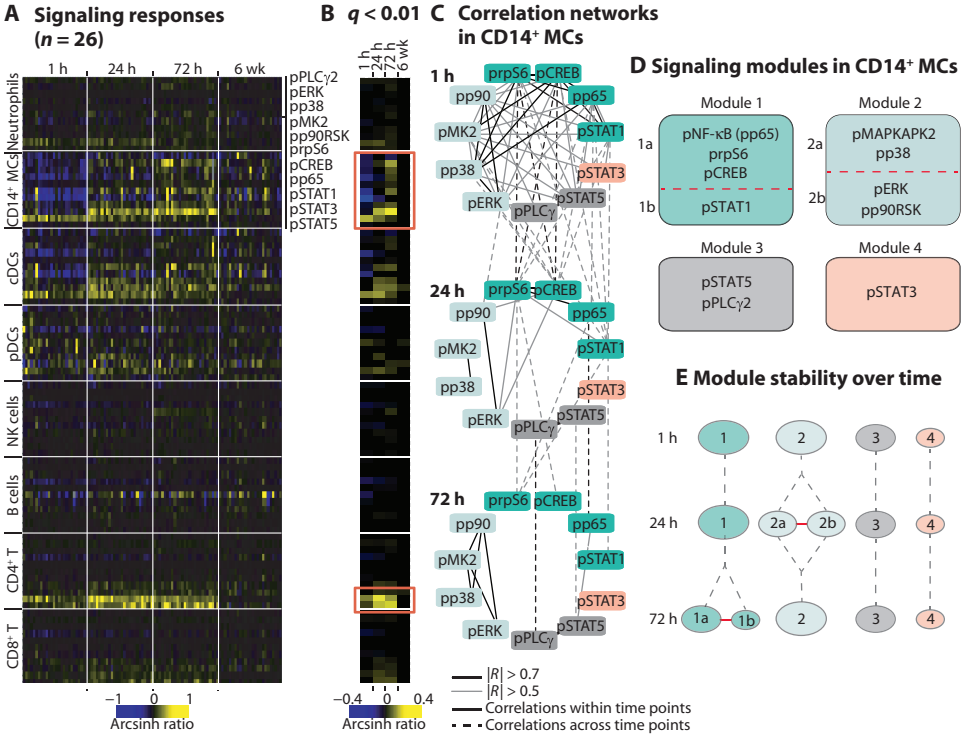

Fig. 3. Surgery induces time-dependent and cell type–specific activation of immune signaling networks. (**A**) Heat map depicting hand-gated major immune cell subsets (rows, fig. S3) and sampling times after surgery (columns). Within each block, changes in phosphorylation state of 11 intracellular signaling proteins (*y* axis) are individually depicted for 26 patients (*x* axis). The color scale indicates changes in phospho-signal median intensity (arcsinh ratio) compared to baseline. (**B**) Heat map depicting each signaling protein, cell subset, and time point whether phosphorylation signals significantly increased (yellow, $q < 0.01$, $n = 26$, SAM two-class paired), decreased (blue, $q < 0.01$), or remained unchanged (black, $q > 0.01$). The color scale indicates mean fold change of the signaling responses compared to baseline. Signaling responses in $CD14^+$ MCs and $CD4^+$ T cells were most prominent (red). (**C**) Pearson correlation coefficients between changes in phosphorylation states of 11 signaling proteins in $CD14^+$ MCs at 1, 24, and 72 hours after surgery were determined. Correlations within each (solid lines) and across (dash lines) time point(s) are depicted as black ($|R| > 0.7$) and gray lines ($|R| > 0.5$). (**D**) Signaling modules in $CD14^+$ MCs at 1, 24, and 72 hours were identified by cutting the dendrograms of clustered correlation coefficients (fig. S8) using a threshold of $R > 0.7$. (**E**) Module stability over time. At 72 hours, module 1 split into modules 1a (pNF-κB, prpS6, pCREB) and 1b (pSTAT1) that correlate ($R = 0.46$, red line). At 24 hours, module 2 split into modules 2a (pMAPKAPK2, pp38) and 2b (pERK, pp90RSK) that correlate ($R = 0.45$, red line).

modules; the pSTAT3 response may be linked to the known increase in plasma IL-6 concentration after surgery (*11*).

Considering that the inflammatory response to surgical trauma can engage as many as 40 receptors including receptors for alarmins (such as TLR2 and TLR4), IL receptors, and others (*8*, *9*), the consistent integration of multiple environmental signals into cell type–specific signaling networks highlights the ability of the immune system to mount a uniform surgical immune response. The magnitude of this response varied among patients, which begs the question as to whether the variability between patients constitutes "noise" or, alternatively, reflects patient-specific differences that could correlate with differences in clinical recovery.

Dense longitudinal characterization of clinical recovery reveals large interpatient variability

Fatigue, pain, and resulting functional impairment after surgery critically determine when patients can resume normal activities and return to work (*5*). Fatigue, pain, and functional impairment of the hip were assessed with the Surgical Recovery Scale (SRS) and adapted versions of the Western Ontario and McMaster Universities Arthritis Index (WOMAC) pain and function subscales. Assessments were obtained daily during hospitalization, and then every third day up to 6 weeks to infer the rate at which individual patient's recovered from surgery. Rates were quantified as the time required to reach half-maximum recovery from fatigue, to transition from moderate to mild pain, and to transition from moderate to mild functional impairment of the hip, all considered to be clinically important milestones in a patient's recovery.

Heat maps depicting parameters of clinical recovery for individual patients during the 6-week period after surgery reflect large interpatient variability for the three outcomes: fatigue, hip function, and pain (Fig. 4, A to C). The median time to recuperate from postoperative fatigue was 3 weeks. Clinical resolution of substantial functional impairment of the hip (score ≤18) and pain (score ≤12) occurred during the second week (Fig. 4, D to F). However, the rate of recovery varied greatly among patients. The median time to regain 50% of recovery from postoperative fatigue was 10 days, with a range of 0 to 36 days. The median time to experience only mild functional impairment of the hip was 15 days, with a range of 2 to 42 days. The median time to suffer from only mild pain was 10 days, with a similar wide range of 2 to 36 days (Fig. 4, G to I). Among all demographic and clinical variables, only gender was significantly related to a clinical recovery parameter. The median time to regain 50% recovery from postoperative fatigue was 6 days (range, 5 to 12) in women and 15 days (range, 6 to 20) in men ($P = 0.02$). Recovery of postoperative fatigue was not correlated with times to mild functional impairment of the hip or pain, but a significant correlation was detected between the times to mild functional impairment of the hip and pain ($R = 0.6$, $P = 0.004$). Thus, in this homogeneous patient population, rates of recovery differed greatly.

Signaling responses in CD14$^+$ MC subsets correlate with surgical recovery

To gain an objective view of the relationships between the multidimensional mass cytometry data set and clinical outcomes, the Citrus method for unsupervised identification of cellular responses associated with a clinical outcome was used (*24*) (Fig. 5A). This algorithm demarks cell subsets using the hierarchical clustering described above (Fig. 2), attributes immune features (cell frequencies and signaling responses) to each cell cluster, and identifies significant associations ($q < 0.01$) between immune features and parameters of clinical recovery using SAM. Significant correlations were detected for six immune cell features at an FDR of 1% ($R = 0.66$ to 0.80, table S3). All were signaling responses in CD14$^+$ MC subsets (Fig. 5, B and C). For instance, changes in STAT3 signaling between 1 and 24 hours in CD14$^+$HLA-DR$^{low/mid}$ MC clusters strongly correlated ($R = 0.72$ to 0.80) with time to 50% recovery from postoperative fatigue (Fig. 5B, panel 1, and fig. S9). Changes in CREB signaling between baseline and 1 hour in the CD14$^+$HLA-DR^{low} MC cluster strongly correlated ($R = 0.66$) with time to mild functional impairment of the hip (Fig. 5B, panel 2). Changes in NF-κB signaling between baseline and 1 hour in the CD14$^+$HLA-DR^{hi} MC cluster strongly correlated ($R = 0.71$) with time to mild pain (Fig. 5B, panel 3). These correlations remained significant and unchanged when accounting for potential confounders [including sex, age, body mass index (BMI), type of anesthesia, duration of surgery, and estimated blood loss; table S4] and were confirmed by a manual gating strategy (Fig. 5, C and D). Because analgesic consumption and pain are interrelated factors, a quantitative analysis accounting for confounding influences of postoperative analgesic consumption on pain was performed (*33*). Variation in analgesic consumption did not alter the correlation between NF-κB signaling in CD14$^+$HLA-DR^{hi} MCs and time to mild pain. Thus, specific signaling responses in monocyte compartments are hallmarks of critical phenotypes defining clinical recovery and account for 40 to 60% of observed interpatient variability.

DISCUSSION

This study applied mass cytometry to survey with single-cell resolution the phenotypic and functional alterations of the human immune system in patients undergoing major surgeries, namely, hip arthroplasty. Simultaneous assessment of immune cell distributions and corresponding intracellular signaling events revealed uniform responses across patients, thereby demarcating a surgical immune signature. Engrained in this immune signature were strong correlates ($R = 0.7$ to 0.8, FDR < 0.01), relating the magnitude of cell type–specific signaling responses to an individual patient's clinical recovery profile.

Mass cytometry provided high-dimensional numerical and functional characterization of the immune response to surgical trauma and enabled the detection of biological mechanisms critically associated with a health-relevant outcome. With an unsupervised algorithmic approach, changes in cell frequencies and immune signaling responses at the single-cell level were systematically evaluated via deep immune system profiling to identify immune correlates of clinical recovery. Two themes evolved: (i) strong correlations were identified with signaling responses but not with changes in cell frequency and (ii) signaling responses that correlated most significantly with clinical recovery occurred in CD14$^+$ MCs. These included changes in STAT3, CREB, and NF-κB activation states within CD14$^+$ MC subsets, which correlated with recovery from fatigue, functional impairment of the hip, and pain after surgery and accounted for 40 to 60% of observed patient variability.

The simultaneous monitoring of major immune cell subsets provided a global view of surgery-induced alterations across the immune system that included precisely timed changes in immune cell distribution and mobilization of distinct signaling networks in innate and adaptive compartments. Consistent with previous studies (*10*, *12*, *22*),

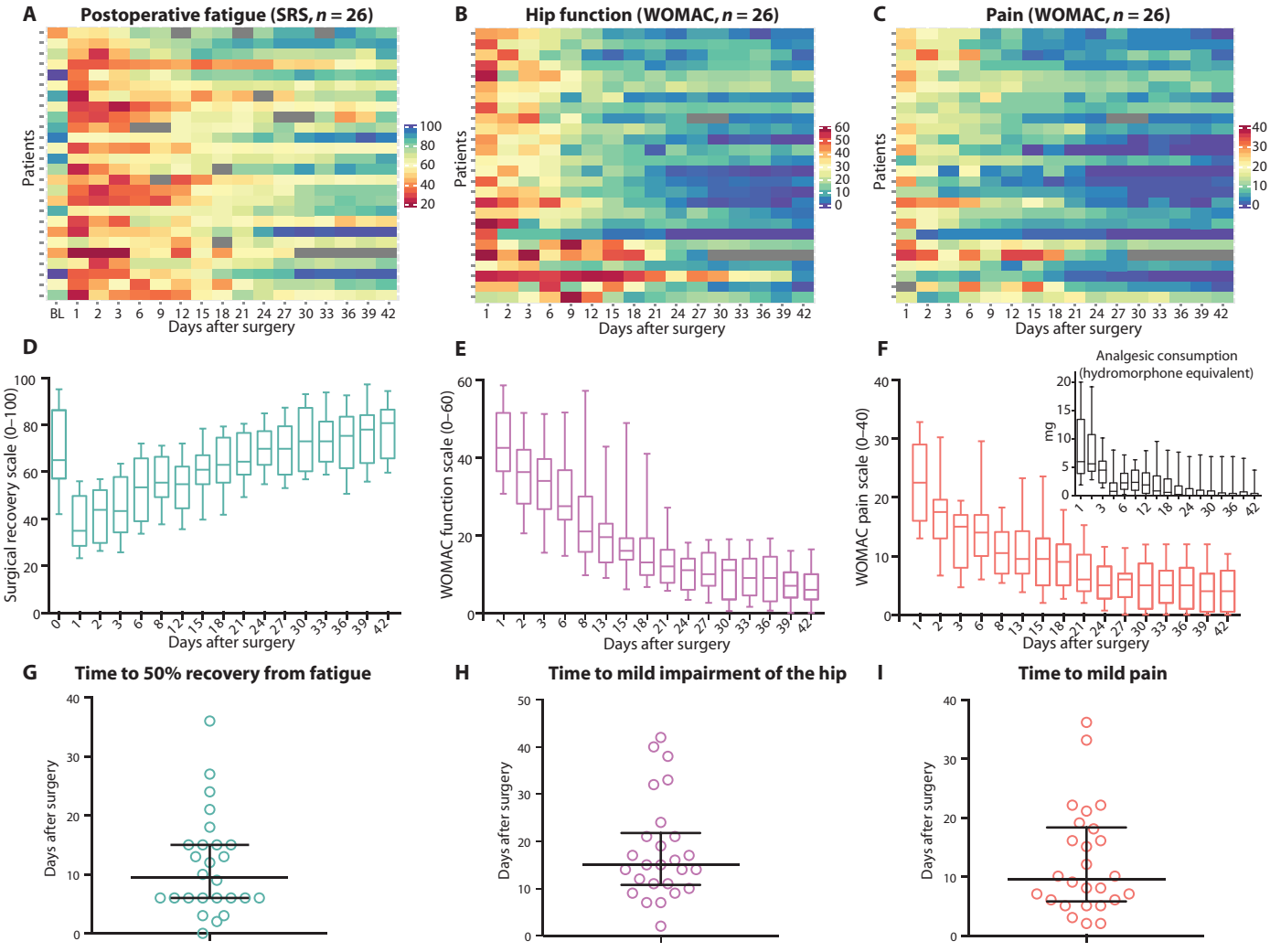

Fig. 4. The rate of surgical recovery varies greatly among patients. (**A** to **C**) Heat maps depict the recovery parameters (A) postoperative fatigue, (B) hip function, and (C) pain for individual patients over the 6-week observation period. Postoperative fatigue was assessed with the SRS (0 to 100 = worst to best function) (*49*). Pain and impairment of hip function were assessed with adapted versions of the WOMAC (pain 0 to 40 = no pain to worst imaginable pain; function 0 to 60 = no impairment to severe functional impairment) (*46*). (**D** to **F**) Box plots depict medians and interquartile ranges of (D) SRS, (E) WOMAC function, and (F) WOMAC pain scores (bars indicate 10th and 90th percentiles, $n = 26$). An inset graph in (F) depicts the median daily analgesic consumption expressed as the dose equivalent of intravenous hydromorphone. Graphical information regarding pain and analgesic consumption are jointly presented because these variables are interdependent. (**G** to **I**) Clinical recovery parameters were derived to quantify rate of recovery for the three outcomes. Derived parameters were (G) time to 50% recovery from postoperative fatigue, (H) time to mild functional impairment of the hip, and (I) time to mild pain. Bars indicate median and interquartile range; open circles indicate individual data points ($n = 26$).

innate immune cells expanded soon after surgery, followed by a reduction of cells within the adaptive branch. In contrast, cell signaling responses occurred early and simultaneously within both immune branches. For instance, orchestrated changes in STAT3 and STAT5 signaling manifested within 1 hour after surgery in $CD14^+$ MCs and $CD4^+$ and $CD8^+$ T cells. Our results challenge the view that innate immune responses to trauma precede adaptive responses. It raises the question of whether adaptive immune cells might migrate to sites to prepare for events driven by innate processes. Our data dovetail with findings of a recent genome-wide analysis of the leukocyte response to major trauma (*13*). In that study, up-regulation of genes associated with the innate immune branch and those encoding proinflammatory mediators, including STAT target genes, was concurrent with the suppression of genes associated with the adaptive immune branch including genes regulating T cell proliferation, antigen presentation, and apoptosis.

In $CD14^+$ MCs, STAT3 phosphorylation peaked 1 hour after surgery in all patients and coincided with the dephosphorylation of 10 signaling proteins, which formed four distinct modules. The observed activation of STAT proteins in $CD14^+$ MCs within 24 hours after surgery is consistent with previously reported trauma-induced increases in plasma cytokine IL-6 (*11*) and IL-10 (*34*), a key response to trauma. Unexpectedly, a biphasic response of several signaling pathways downstream of TLRs, which play a major role in innate immunity (*28*, *29*), was observed. This might be due to the release of trauma-induced signaling molecules such as HMGB1, heat shock proteins, and other alarmins known to act on TLRs and other immune mediators of inflammation

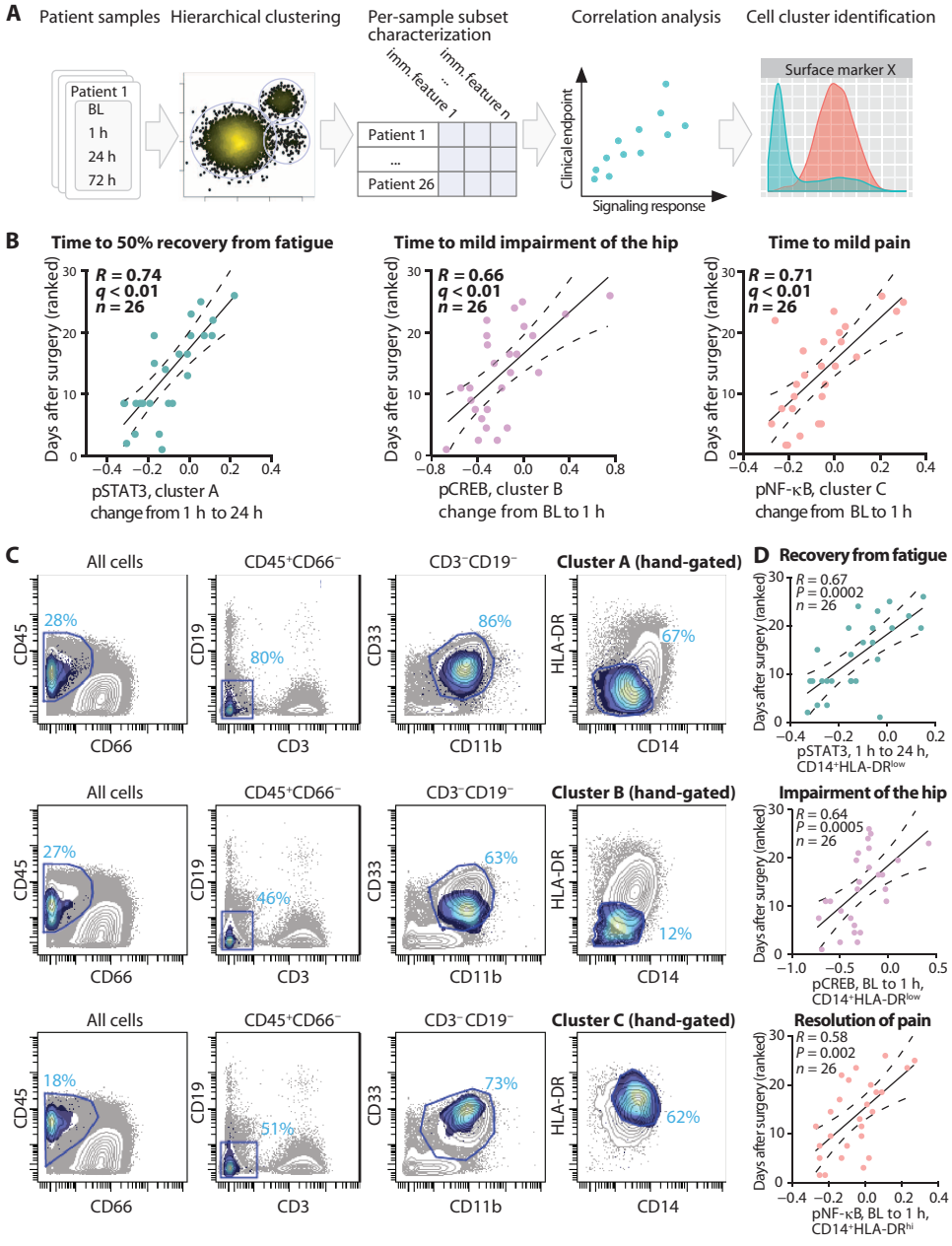

Fig. 5. STAT3, CREB, and NF-κB signaling in CD14$^+$ MC subsets correlate with surgical recovery. (**A**) CD45$^+$CD66$^-$ cells obtained at baseline and at 1, 24, and 72 hours after surgery were clustered using an unsupervised approach (*24*) (panels 1 and 2, Fig. 3B). Immune features, which include frequencies and signaling responses of 11 phospho-proteins, were derived for every cluster (panel 3). SAM quantitative method was used to detect significant correlations between immune features and parameters of clinical recovery (q < 0.01, n = 26, panel 4). Cell cluster phenotypes were identified using cell surface marker expression (panel 5). (**B**) Significant correlations of STAT3 signaling in cluster A (left panel), CREB signaling in cluster B (middle panel), and NF-κB signaling in cluster C (right panel) with recovery from postoperative fatigue, functional impairment of the hip, and resolution of pain. Clusters A and B were CD14$^+$HLA-DR^{low} MCs; cluster C was CD14$^+$HLA-DR^{hi} MCs (fig. S9). (**C**) Cells were hand-gated using 12 surface markers (blue line). Representative two-dimensional plots are shown for one patient at 24 hours (upper panel) and 1 hour (middle and lower panels) after surgery. Percent cells in parent gate are shown. Cells contained in clusters A, B, and C (blue shadow) are overlaid onto the entire cell population (gray). (**D**) Significant correlations between signaling responses and parameters of clinical recovery identified using an unsupervised approach were replicated with hand-gated data. Depicted are regression lines and 95% confidence intervals (solid and dashed lines), Spearman's ranked correlation coefficients, FDRs (q), and P values (n = 26).

(*8*, *35*). The coordinated and sequential dephosphorylation and phosphorylation of these proteins are reminiscent of oscillations in NF-κB nuclear translocation, which control the expression of NF-κB target genes (*36*). Oscillations in CREB and NF-κB signaling networks together with STAT3 signaling may drive the response of CD14$^+$ MCs to surgical trauma.

Observed similarities in signaling activities among patients are indicative of a tightly regimented immune response to surgical trauma. We hypothesized that the differences in the magnitude of such responses may account for differences in recovery from surgery. Indeed, interpatient variability in phosphorylation of proteins within two signaling modules in CD14$^+$ MCs, those involving STAT3 (module 4) and CREB and NF-κB (module 1), strongly correlated with recovery from postoperative fatigue and resolution of pain after surgery, suggesting that differential engagement of these signaling networks in CD14$^+$ MCs regulates important aspects of clinical recovery.

The most significant immune correlates of clinical recovery occurred in CD11b$^+$CD14$^+$HLA-DR^{low} monocytes. A marked overrepresentation of this cell subset was observed at 24 and 72 hours after surgery. An explanation that could account for this observation is the down-regulation of HLA-DR expression, a proposed mechanism of "monocytic anergy" after major trauma and sepsis (*37*, *38*). However, phenotypically, the CD11b$^+$CD14$^+$HLA-DR^{low} monocytes we observed are remarkably similar to that reported for MDSCs, which markedly expand in a mouse model of surgery (*39*). In human malignancies, CD11b$^+$CD14$^+$HLA-DR^{low} MDSCs proliferate and suppress T cell responses in a STAT3-dependent fashion (*25*, *40*). The observed preponderance of CD11b$^+$CD14$^+$HLA-DR^{low} cells after surgery and the strong correlation between STAT3 signaling in these cells and patients' fatigue suggest that these cells might play an important role in regulating critical aspects of clinical recovery.

Previous studies had revealed a link between surgery-related inflammatory responses and clinical recovery; however, the immune features only explained a small fraction of variability in recovery rates and provided limited mechanistic insight. For example, Hall *et al.* detected

a correlation between IL-6 plasma concentrations at 24 hours after hip replacement and the time after surgery when a patient was able to walk 25 m (*41*). Rosenberg *et al.* found a correlation between leukocyte redistribution from the bloodstream and joint function after surgery in patients undergoing knee replacement (*10*). By contrast, the study presented here revealed highly specific immune correlates accounting for 40 to 60% of variability in recovery rates. Previous studies that relied on bulk analysis, precluded detailed subsetting of cells, or could not measure functional attributes of rare cell subsets may have missed strong correlative signals. Notably, in our study, signaling responses in less than 2% of peripheral leukocytes correlated with a given clinical correlate.

This study has certain limitations. The patient cohort, although homogeneous, suffered from minimal comorbidities and underwent the same surgical procedure, which enabled the identification of key immune correlates of recovery from hip surgery. These results may not extrapolate to all types of surgery or trauma, but the highly structured immune response observed in these patients suggests that reported immune signatures might be generalizable. Our study was therefore designed to ask "what were the baseline immune correlates for this type of surgery." We expect of course that comorbidities might introduce additional variations specific to the copathology. The immune correlates of clinical recovery were derived from the analysis of samples collected within 72 hours after surgery, leaving open the possibility that other important and identifiable events may occur later in the recovery phase. Finally, whereas the relevant signaling events identified in the pilot study were subsequently validated in a 26-patient cohort, the predictive value of observed clinical recovery correlates will require prospective validation in an independent patient cohort.

The role of monocytes in surgical recovery and trauma has been the subject of substantial interest (*26*, *42*–*45*). Application of single-cell analysis at the bedside enabled identification of strong and specific immune correlates in $CD14^+$ MCs that accounted for 40 to 60% of patient-associated variability in recovery after PHA. Immune correlates pertained to the functional (that is, signaling) state of $CD14^+$ MCs rather than their frequency. These data provide a set of mechanistically derived immune features for the development of a diagnostic test predicting clinical recovery after PHA. Future studies hold promise for the identification of immune correlates of patient recovery in the context of other traumatic injuries such as orthopedic as well as non-orthopedic surgeries, accidental injuries, and military traumas.

MATERIALS AND METHODS

Study design

Subjects. The study was approved by the Institutional Review Board of Stanford University School of Medicine and registered with ClinicalTrials.gov (NCT01578798). Patients scheduled for PHA for nontraumatic osteoarthritis were recruited from the Arthritis and Joint Replacement Clinic in the Department of Orthopedic Surgery at Stanford University School of Medicine. Hip arthroplasties were performed by one of three surgeons using a standard lateral approach, wound drains, and compression dressings. Anesthetic management consisted of a general inhalation anesthesia supplemented with opiate-based analgesia. Unless counter-indicated, patients were offered a spinal anesthetic. Hospital discharge was planned for postoperative days 3 to 4. A total of 251 patients were screened, 81 were approached for informed consent, 50 were consented, 39 were actively enrolled, and 32 completed the study (fig. S2 and Table 1).

Study protocol. Assessments were made 1 hour before and 1, 24, 48, and 72 hours after surgery and every third day from day 6 to day 42. Clinical outcomes were captured with the SRS (0 to 100 = worst to best function), an adapted WOMAC pain scale (WOMAC-P; 0 to 40 = no pain to worst imaginable pain), and an adapted WOMAC function scale (WOMAC-F; 0 to 60 = no impairment to severe functional impairment). Adapted versions were used because not all questions applied to the postoperative setting. Daily opioid consumption was captured as intravenous hydromorphone equivalents. Full versions of the WOMAC, the Short Form Health Survey (SF-36), the Profile of Moods States Tension-Anxiety Scale (POMS-A), and the Beck Depression Inventory (BDI) were completed at the beginning and end of the study (*46*–*49*).

Clinical data. Recovery from postoperative fatigue (SRS) was quantified as the time required to half-maximum recovery (SRS-$t_{1/2}$), defined by a surgical recovery index (SRI) equivalent to the sum of the minimum SRI after surgery and half of the difference between the preoperative SRI and the minimum SRI. SRS-$t_{1/2}$ represents substantial clinical improvement in five key descriptors of postoperative fatigue: feelings of fatigue, feelings of vigor, impacts on concentration, impacts on energy, and impacts on daily activities. SRS-$t_{1/2}$ was more sensitive than time to full recovery because the latter parameter was affected by ceiling effects.

Recovery from pain was quantified as the time required to achieve a WOMAC-P $\leq$12 (T_{12}). WOMAC-P was composed of four scores (0 to 10 = no pain to most imaginable pain) to quantify pain at night, at rest, when bearing weight, and during walking. A cumulative score of 12 indicates transition from mild to moderate pain across the conditions (*50*).

Recovery of hip function was quantified as the time required to achieve a WOMAC-F $\leq$18 (T_{18}). WOMAC-F was composed of six scores (0 to 10 = no to severely impaired) to quantify function in the affected hip when lying in bed, rising from bed, sitting, rising from sitting, standing, and walking on flat surface. A cumulative score of 18 indicates transition from moderate to mild functional impairment, reflecting substantial improvement in a patient's ability to perform functional tasks involving the hip joint.

Sample size determination for the validation of surgery-induced signaling events. A power analysis was anchored in the pilot data (six patients, Fig. 1). Considering all signaling responses with arcsinh ratios equal or greater than 0.2, the response associated with the highest variance (pp38 in $CD14^+$ MCs) was used to determine power. Assuming an α level of 0.001, a sample size of 24 patients would allow detecting this signaling response with a power of 90%.

Patient sample processing by mass cytometry

Whole-blood processing. Blood samples were fixed using a fixation/stabilization buffer (Smart Tube Inc.) within 30 min of phlebotomy and stored at −80°C. Samples were thawed on the day of processing. Red blood cells were lysed using a hypotonic buffer (Smart Tube Inc.). Peripheral blood leukocytes were washed and resuspended in cell staining medium.

Antibodies. Antibodies were chosen to facilitate the identification of major immune cell types in whole blood (fig. S3) and to measure immune signaling pathways likely to be affected by surgery. The antibodies used for the six-patient pilot study are listed in table S1, a subset of these were used for experiments described in fig. S1.

Cell barcoding and antibody staining. Time points from the same patient (baseline, 1 hour, 24 hours, 72 hours, and 6 weeks) were barcoded and processed simultaneously for antibody staining (Supplementary Materials and Methods). Therefore, each of a given patient's time points was subjected to identical processing, such that there was no systematic experimental bias applied to a given time point across patients. To protect against potential batch effects, all findings are quantified as relative changes between time points (that is, all reported values are normalized to a signal from its same barcode plate). Machine-based batch effects were normalized after processing (*21*).

All decisions regarding which patients were barcoded together, and all staining, mass cytometry analysis, and quantification of changes were performed blinded to the patients' recovery status. In addition, immune features used for regression against recovery were derived blinded to recovery indices.

Mass cytometry. Stained cells were analyzed on a mass cytometer (CyTOF, DVS Sciences) at an event rate of 400 to 500 cells per second. Data files for each barcoded sample were concatenated using an in-house script. The data were normalized using Normalizer v0.1 MCR (*21*). Files were debarcoded using the Matlab Debarcoder Tool. Gating was performed in http://nolanlab.cytobank.org (fig. S3).

Mass cytometry data processing. An inverse hyperbolic sine transformation was applied to analyze protein phosphorylation data. The difference of the median of the transformed values between baseline and 1 hour, 24 hours, 72 hours, and 6 weeks after surgery is reported as the arcsinh ratio.

Statistical analysis

Statistical analyses of molecular parameters. Significant changes in cell frequency and phosphorylation state were inferred with SAM (*27*), using the "samr" package in R. SAM is a nonparametric test that assigns a score to the change in each feature, and thresholds that score for significance based on an estimate of FDR derived from permuting the observed data. This test was selected because it considers multiple-hypothesis testing, makes few assumptions about the distribution of the underlying data, and has been validated for use on high-dimensional biological data. SAM two-class paired was performed for hand-gated data. Significance was inferred for an FDR <1% ($q < 0.01$).

Correlation network analysis. Monocyte signaling responses from all time points were used to generate a Pearson correlation matrix, which was clustered using single-linkage clustering (fig. S8). Clusters were collapsed into a module when the within-cluster correlation exceeded 0.7 (Fig. 3D). Correlations between two modules were calculated as the average of the correlation between the points in the two modules (Fig. 3E).

Clustering. Hierarchical clustering using Ward's linkage and Euclidean distance was performed as described by Bruggner *et al.* (*24*) on $CD45^+CD66^-$ cells using R (Figs. 2 and 5). Cells were clustered on the basis of the expression of CD7, CD19, CD11b, CD4, CD8, CD127, CCR7, CD123, CD45RA, CD33, CD11c, CD14, CD16, FoxP3, CD25, CD3, HLA-DR, and CD56. Ten thousand events were sampled from each patient sample for clustering. Clusters containing at least 1% of all clustered cells are graphically displayed. Cluster plots depict the clustering hierarchy, and nodes are scaled on the basis of frequency of cells in that cluster. Data from time points that were included in the same SAM analysis were clustered together to enable comparison of clusters between time points.

Correlation analyses of molecular and clinical parameters. Correlation analyses of molecular features derived from mass cytometry data and clinical parameters were performed using Citrus, a method for unsupervised identification of cellular responses associated with a clinical outcome (*24*). Briefly, cell subsets were identified using hierarchical clustering as described in the Clustering section. Cells from each patient and from each time point were pooled for clustering to enable comparison across samples. For each cluster in each patient, cluster abundances and the median value of 11 phospho-proteins were calculated as relative changes between time points to avoid potential batch effects. Associations between clinical endpoints and cluster properties were identified using the SAM quantitative method. Repeated runs of the analysis with identical parameters confirmed that results were reproducible.

Partial correlation was performed by correlating the residuals from (i) the correlation of the clinical covariate with the immune feature and (ii) the correlation between the clinical covariate and the clinical index. Clinical covariates included age, sex, BMI, estimated blood loss, length of surgery, use of regional anesthesia, and baseline clinical indices of recovery. Analysis was performed in the R software environment. *P* values from this analysis were compared to the *P* values for the immune feature correlation with the clinical index and are listed in table S4.

SUPPLEMENTARY MATERIALS

www.sciencetranslationalmedicine.org/cgi/content/full/6/255/255ra131/DC1
Materials and Methods
Fig. S1. Assay performance and validation.
Fig. S2. Consort chart summarizes patient recruitment.
Fig. S3. Manual gating strategy.
Fig. S4. Changes in cell frequencies in serial samples from the six patients included in the pilot study.
Fig. S5. Annotation of cluster hierarchy plots based on surface marker expression.
Fig. S6. SAM analysis of cell frequency changes across clusters.
Fig. S7. Signaling responses over time in innate and adaptive immune compartments.
Fig. S8. Correlation heat maps and module derivation in $CD14^+$ MCs.
Fig. S9. Immune feature correlations and identification of clusters A1, A2, and A3.
Table S1. Antibody panels used for mass cytometry analysis.
Table S2. SAM analysis of intracellular signaling responses over time.
Table S3. Immune features correlating with clinical parameters of surgical recovery.
Table S4. Immune feature correlations with clinical parameter of surgical recovery corrected for clinical covariates.

REFERENCES AND NOTES

1. T. G. Weiser, S. E. Regenbogen, K. D. Thompson, A. B. Haynes, S. R. Lipsitz, W. R. Berry, A. A. Gawande, An estimation of the global volume of surgery: A modelling strategy based on available data. *Lancet* **372**, 139–144 (2008).
2. H. Kehlet, J. B. Dahl, Anaesthesia, surgery, and challenges in postoperative recovery. *Lancet* **362**, 1921–1928 (2003).
3. R. Allvin, K. Berg, E. Idvall, U. Nilsson, Postoperative recovery: A concept analysis. *J. Adv. Nurs.* **57**, 552–558 (2007).
4. L. Lee, T. Tran, N. E. Mayo, F. Carli, L. S. Feldman, What does it really mean to "recover" from an operation? *Surgery* **155**, 211–216 (2014).
5. T. Bisgaard, M. Støckel, B. Klarskov, H. Kehlet, J. Rosenberg, Prospective analysis of convalescence and early pain after uncomplicated laparoscopic fundoplication. *Br. J. Surg.* **91**, 1473–1478 (2004).
6. T. Bisgaard, B. Klarskov, J. Rosenberg, H. Kehlet, Factors determining convalescence after uncomplicated laparoscopic cholecystectomy. *Arch. Surg.* **136**, 917–921 (2001).
7. M. Adamina, H. Kehlet, G. A. Tomlinson, A. J. Senagore, C. P. Delaney, Enhanced recovery pathways optimize health outcomes and resource utilization: A meta-analysis of randomized controlled trials in colorectal surgery. *Surgery* **149**, 830–840 (2011).
8. V. M. Stoecklein, A. Osuka, J. A. Lederer, Trauma equals danger—Damage control by the immune system. *J. Leukoc. Biol.* **92**, 539–551 (2012).

9. U. Andersson, K. J. Tracey, HMGB1 is a therapeutic target for sterile inflammation and infection. *Annu. Rev. Immunol.* **29**, 139–162 (2011).
10. P. H. Rosenberger, J. R. Ickovics, E. Epel, E. Nadler, P. Jokl, J. P. Fulkerson, J. M. Tillie, F. S. Dhabhar, Surgical stress-induced immune cell redistribution profiles predict short-term and long-term postsurgical recovery. A prospective study. *J. Bone Joint Surg. Am.* **91**, 2783–2794 (2009).
11. R. J. Baigrie, P. M. Lamont, D. Kwiatkowski, M. J. Dallman, P. J. Morris, Systemic cytokine response after major surgery. *Br. J. Surg.* **79**, 757–760 (1992).
12. M. S. Slade, R. L. Simmons, E. Yunis, L. J. Greenberg, Immunodepression after major surgery in normal patients. *Surgery* **78**, 363–372 (1975).
13. W. Xiao, M. N. Mindrinos, J. Seok, J. Cuschieri, A. G. Cuenca, H. Gao, D. L. Hayden, L. Hennessy, E. E. Moore, J. P. Minei, P. E. Bankey, J. L. Johnson, J. Sperry, A. B. Nathens, T. R. Billiar, M. A. West, B. H. Brownstein, P. H. Mason, H. V. Baker, C. C. Finnerty, M. G. Jeschke, M. C. López, M. B. Klein, R. L. Gamelli, N. S. Gibran, B. Arnoldo, W. Xu, Y. Zhang, S. E. Calvano, G. P. McDonald-Smith, D. A. Schoenfeld, J. D. Storey, J. P. Cobb, H. S. Warren, L. L. Moldawer, D. N. Herndon, S. F. Lowry, R. V. Maier, R. W. Davis, R. G. Tompkins; Inflammation and Host Response to Injury Large-Scale Collaborative Research Program, A genomic storm in critically injured humans. *J. Exp. Med.* **208**, 2581–2590 (2011).
14. D. W. Wilmore, From Cuthbertson to fast-track surgery: 70 years of progress in reducing stress in surgical patients. *Ann. Surg.* **236**, 643–648 (2002).
15. M. W. Wichmann, T. P. Hüttl, H. Winter, F. Spelsberg, M. K. Angele, M. M. Heiss, K. W. Jauch, Immunological effects of laparoscopic vs open colorectal surgery: A prospective clinical study. *Arch. Surg.* **140**, 692–697 (2005).
16. E. Lin, S. E. Calvano, S. F. Lowry, Inflammatory cytokines and cell response in surgery. *Surgery* **127**, 117–126 (2000).
17. S. Reinke, S. Geissler, W. R. Taylor, K. Schmidt-Bleek, K. Juelke, V. Schwachmeyer, M. Dahne, T. Hartwig, L. Akyuz, C. Meisel, N. Unterwalder, N. B. Singh, P. Reinke, N. P. Haas, H. D. Volk, G. N. Duda, Terminally differentiated $CD8^+$ T cells negatively affect bone regeneration in humans. *Sci. Transl. Med.* **5**, 177ra136 (2013).
18. Z. B. Bjornson, G. P. Nolan, W. J. Fantl, Single-cell mass cytometry for analysis of immune system functional states. *Curr. Opin. Immunol.* **25**, 484–494 (2013).
19. B. Bodenmiller, E. R. Zunder, R. Finck, T. J. Chen, E. S. Savig, R. V. Bruggner, E. F. Simonds, S. C. Bendall, K. Sachs, P. O. Krutzik, G. P. Nolan, Multiplexed mass cytometry profiling of cellular states perturbed by small-molecule regulators. *Nat. Biotechnol.* **30**, 858–867 (2012).
20. S. C. Bendall, E. F. Simonds, P. Qiu, A. D. Amir el, P. O. Krutzik, R. Finck, R. V. Bruggner, R. Melamed, A. Trejo, O. I. Ornatsky, R. S. Balderas, S. K. Plevritis, K. Sachs, D. Pe'er, S. D. Tanner, G. P. Nolan, Single-cell mass cytometry of differential immune and drug responses across a human hematopoietic continuum. *Science* **332**, 687–696 (2011).
21. R. Finck, E. F. Simonds, A. Jager, S. Krishnaswamy, K. Sachs, W. Fantl, D. Pe'er, G. P. Nolan, S. C. Bendall, Normalization of mass cytometry data with bead standards. *Cytometry A* **83**, 483–494 (2013).
22. C. S. Ho, J. A. López, S. Vuckovic, C. M. Pyke, R. L. Hockey, D. N. Hart, Surgical and physical stress increases circulating blood dendritic cell counts independently of monocyte counts. *Blood* **98**, 140–145 (2001).
23. H. T. Maecker, J. P. McCoy, R. Nussenblatt, Standardizing immunophenotyping for the Human Immunology Project. *Nat. Rev. Immunol.* **12**, 191–200 (2012).
24. R. V. Bruggner, B. Bodenmiller, D. L. Dill, R. J. Tibshirani, G. P. Nolan, Automated identification of stratifying signatures in cellular subpopulations. *Proc. Natl. Acad. Sci. U.S.A.* **111**, E2770–E2777 (2014).
25. I. Poschke, D. Mougiakakos, J. Hansson, G. V. Masucci, R. Kiessling, Immature immunosuppressive $CD14^+HLA\text{-}DR^{-/low}$ cells in melanoma patients are $Stat3^{hi}$ and overexpress CD80, CD83, and DC-sign. *Cancer Res.* **70**, 4335–4345 (2010).
26. C. H. Wakefield, P. D. Carey, S. Foulds, J. R. Monson, P. J. Guillou, Changes in major histocompatibility complex class II expression in monocytes and T cells of patients developing infection after surgery. *Br. J. Surg.* **80**, 205–209 (1993).
27. V. G. Tusher, R. Tibshirani, G. Chu, Significance analysis of microarrays applied to the ionizing radiation response. *Proc. Natl. Acad. Sci. U.S.A.* **98**, 5116–5121 (2001).
28. J. M. Park, F. R. Greten, A. Wong, R. J. Westrick, J. S. Arthur, K. Otsu, A. Hoffmann, M. Montminy, M. Karin, Signaling pathways and genes that inhibit pathogen-induced macrophage apoptosis—CREB and NF-κB as key regulators. *Immunity* **23**, 319–329 (2005).
29. B. Beutler, Inferences, questions and possibilities in Toll-like receptor signalling. *Nature* **430**, 257–263 (2004).
30. V. Toshchakov, B. W. Jones, P. Y. Perera, K. Thomas, M. J. Cody, S. Zhang, B. R. Williams, J. Major, T. A. Hamilton, M. J. Fenton, S. N. Vogel, TLR4, but not TLR2, mediates IFN-β–induced STAT1α/β-dependent gene expression in macrophages. *Nat. Immunol.* **3**, 392–398 (2002).
31. J. J. O'Shea, R. Plenge, JAK and STAT signaling molecules in immunoregulation and immune-mediated disease. *Immunity* **36**, 542–550 (2012).
32. T. B. Geijtenbeek, S. I. Gringhuis, Signalling through C-type lectin receptors: Shaping immune responses. *Nat. Rev. Immunol.* **9**, 465–479 (2009).
33. F. Dai, D. G. Silverman, J. E. Chelly, J. Li, I. Belfer, L. Qin, Integration of pain score and morphine consumption in analgesic clinical studies. *J. Pain* **14**, 767–777.e8 (2013).
34. P. V. Giannoudis, R. M. Smith, S. L. Perry, A. J. Windsor, R. A. Dickson, M. C. Bellamy, Immediate IL-10 expression following major orthopaedic trauma: Relationship to anti-inflammatory response and subsequent development of sepsis. *Intensive Care Med.* **26**, 1076–1081 (2000).
35. J. K. Chan, J. Roth, J. J. Oppenheim, K. J. Tracey, T. Vogl, M. Feldmann, N. Horwood, J. Nanchahal, Alarmins: Awaiting a clinical response. *J. Clin. Invest.* **122**, 2711–2719 (2012).
36. D. E. Nelson, A. E. Ihekwaba, M. Elliott, J. R. Johnson, C. A. Gibney, B. E. Foreman, G. Nelson, V. See, C. A. Horton, D. G. Spiller, S. W. Edwards, H. P. McDowell, J. F. Unitt, E. Sullivan, R. Grimley, N. Benson, D. Broomhead, D. B. Kell, M. R. White, Oscillations in NF-κB signaling control the dynamics of gene expression. *Science* **306**, 704–708 (2004).
37. W. D. Döcke, F. Randow, U. Syrbe, D. Krausch, K. Asadullah, P. Reinke, H. D. Volk, W. Kox, Monocyte deactivation in septic patients: Restoration by IFN-γ treatment. *Nat. Med.* **3**, 678–681 (1997).
38. R. S. Hotchkiss, S. Opal, Immunotherapy for sepsis—A new approach against an ancient foe. *N. Engl. J. Med.* **363**, 87–89 (2010).
39. V. P. Makarenkova, V. Bansal, B. M. Matta, L. A. Perez, J. B. Ochoa, $CD11b^+/Gr\text{-}1^+$ myeloid suppressor cells cause T cell dysfunction after traumatic stress. *J. Immunol.* **176**, 2085–2094 (2006).
40. T. Condamine, D. I. Gabrilovich, Molecular mechanisms regulating myeloid-derived suppressor cell differentiation and function. *Trends Immunol.* **32**, 19–25 (2011).
41. G. M. Hall, D. Peerbhoy, A. Shenkin, C. J. Parker, P. Salmon, Relationship of the functional recovery after hip arthroplasty to the neuroendocrine and inflammatory responses. *Br. J. Anaesth.* **87**, 537–542 (2001).
42. M. Ditschkowski, E. Kreuzfelder, V. Rebmann, S. Ferencik, M. Majetschak, E. N. Schmid, U. Obertacke, H. Hirche, U. F. Schade, H. Grosse-Wilde, HLA-DR expression and soluble HLA-DR levels in septic patients after trauma. *Ann. Surg.* **229**, 246–254 (1999).
43. T. J. Murphy, H. M. Paterson, J. A. Mannick, J. A. Lederer, Injury, sepsis, and the regulation of Toll-like receptor responses. *J. Leukoc. Biol.* **75**, 400–407 (2004).
44. A. Tárnok, J. Bocsi, M. Pipek, P. Osmancik, G. Valet, P. Schneider, J. Hambsch, Preoperative prediction of postoperative edema and effusion in pediatric cardiac surgery by altered antigen expression patterns on granulocytes and monocytes. *Cytometry* **46**, 247–253 (2001).
45. V. Degos, S. Vacas, Z. Han, N. van Rooijen, P. Gressens, H. Su, W. L. Young, M. Maze, Depletion of bone marrow-derived macrophages perturbs the innate immune response to surgery and reduces postoperative memory dysfunction. *Anesthesiology* **118**, 527–536 (2013).
46. N. Bellamy, W. W. Buchanan, C. H. Goldsmith, J. Campbell, L. W. Stitt, Validation study of WOMAC: A health status instrument for measuring clinically important patient relevant outcomes to antirheumatic drug therapy in patients with osteoarthritis of the hip or knee. *J. Rheumatol.* **15**, 1833–1840 (1988).
47. J. E. Ware Jr., SF-36 health survey update. *Spine* **25**, 3130–3139 (2000).
48. A. T. Beck, R. A. Steer, Internal consistencies of the original and revised Beck Depression Inventory. *J. Clin. Psychol.* **40**, 1365–1367 (1984).
49. J. S. Paddison, T. Sammour, A. Kahokehr, K. Zargar-Shoshtari, A. G. Hill, Development and validation of the Surgical Recovery Scale (SRS). *J. Surg. Res.* **167**, e85–e91 (2011).
50. M. P. Jensen, C. Chen, A. M. Brugger, Interpretation of visual analog scale ratings and change scores: A reanalysis of two clinical trials of postoperative pain. *J. Pain* **4**, 407–414 (2003).

Acknowledgments: We thank R. Tibshirani for the critical reading of the manuscript. We also thank A. Trejo and A. Jager for technical support with the CyTOF and antibody labeling. **Funding:** Supported by funds from NIH T32GM089626 and the Stanford Society of Physician Scholars grant (B.G.); the Stanford Bio-X graduate research fellowship and NIH T32GM007276 (G.K.F.); NIH 5T15LM007033-27 (R.V.B.); the Damon Runyon Cancer Research Foundation Fellowship (DRG-2017-09) and NIH 1K99GM104148-01 (S.C.B.); the Food and Drug Administration Contract HHSF223201210194C and National Cancer Institute U54 CA149145 (M.N.); and the Stanford Department of Anesthesiology, Perioperative and Pain Medicine (M.S.A.). G.P.N. is supported by funds from NIH grants UL1RR025744, 1R01CA130826, 5U54CA143907, HHSN272200700038C, N01-HV-00242, 41000411217, 1U19AI100627, P01CA034233-22A1, U19AI057229, U54CA149145, and S10RR027582-01; the California Institute for Regenerative Medicine (DR1-01477 and RB2-01592); the European Commission (HEALTH.2010.1.2-1); and the U.S. Department of Defense (W81XWH-12-1-0591 OCRP-TIA NWC). **Author contributions:** B.G. and G.K.F. conceived the study, conducted experiments, and wrote the manuscript. R.V.B., M.N., and R.F. developed and assisted in the implementation of computational methods for statistical data analysis. M.T. and J.S. assisted in patient recruitment and clinical data collection. E.A.G. and C.G.Y. assisted in the fabrication of reagents and sample processing for mass cytometry analysis. W.J.M., J.I.H., and S.B.G. assisted in clinical study design and patient recruitment. M.M.D. and S.C.B. assisted in experimental design and interpreting data. W.J.F. assisted in interpreting data and writing the manuscript. M.S.A. and G.P.N. conceived and supervised the execution of the study, and wrote the manuscript. **Competing interests:** G.P.N. has personal financial interest in the companies Fluidigm and Becton Dickinson, the manufacturers that produce the reagents or instrumentation used in this manuscript. A provisional patent has

been filed by Stanford University (S13-373, STAN-1069PRV2). Stanford seeks to patent assays that use identified immune features to predict recovery of surgical patients. **Data and materials availability:** The data for this study have been deposited in a public report hosted by cytobank.org (https://www.cytobank.org/cytobank/experiments?project=609).

Submitted 3 June 2014
Accepted 1 August 2014
Published 24 September 2014
10.1126/scitranslmed.3009701

Citation: B. Gaudillière, G. K. Fragiadakis, R. V. Bruggner, M. Nicolau, R. Finck, M. Tingle, J. Silva, E. A. Ganio, C. G. Yeh, W. J. Maloney, J. I. Huddleston, S. B. Goodman, M. M. Davis, S. C. Bendall, W. J. Fantl, M. S. Angst, G. P. Nolan, Clinical recovery from surgery correlates with single-cell immune signatures. *Sci. Transl. Med.* **6**, 255ra131 (2014).

Science Translational Medicine
AAAS

Clinical recovery from surgery correlates with single-cell immune signatures

Brice Gaudillière *et al.*

Sci Transl Med **6**, 255ra131 (2014);
DOI: 10.1126/scitranslmed.3009701

Editor's Summary

Signaling Surgical Recovery

The speed and ease of recovery after surgery differ for every patient, and determining the mechanisms that drive recovery could lead to patient-specific recovery protocols. Gaudilliere *et al.* used mass cytometry to characterize postsurgical immunological insult at a single-cell level and found a surgical immune signature that correlated with clinical recovery across patients. Specifically, cell signaling responses, but not cell frequency, were linked to recovery. Moreover, the correlated signaling responses occurred most notably in $CD14^{+}$ monocytes, suggesting that these cells may play a predominant role in surgical recovery. The consistency of this signature across patients suggests a tightly regulated immune response to surgical trauma, which, if validated, may form the basis of a diagnostic guideline for personalized postsurgical care.

Science Translational Medicine (print ISSN 1946-6234; online ISSN 1946-6242) is published weekly, except the last week in December, by the American Association for the Advancement of Science, 1200 New York Avenue NW, Washington, DC 20005.